Radiative lifetimes, collisional mixing, and quenching of the cesium $5D_J$ levels

A. Sasso* and W. Demtröder
Fachbereich Physik, Universität Kaiserslautern, 6750 Kaiserslautern, Germany

T. Colbert,† C. Wang, E. Ehrlacher, and J. Huennekens
Department of Physics, Building 16, Lehigh University, Bethlehem, Pennsylvania 18015
(Received 26 July 1991)

We report the results of a series of pulsed and cw laser experiments which measure spontaneous and effective lifetimes of the Cs($5D_J$) levels and investigate excitation-transfer collisions involving Cs($5D_J$) atoms and ground-state-cesium perturbers. With cw excitation of the dipole-forbidden but electric-quadrupole-allowed $6S_{1/2}\rightarrow 5D_{5/2}$ transition, we monitor the ratio of sensitized to direct fluorescence, i.e., $I_{5D_{3/2}\rightarrow 6P_{1/2}}/I_{5D_{5/2}\rightarrow 6P_{3/2}}$. A rate-equation analysis of these data yields values for the $\mathrm{Cs}(5D_{5/2})+\mathrm{Cs}(6S)\rightarrow\mathrm{Cs}(5D_{3/2})+\mathrm{Cs}(6S)$ excitation-transfer rate, and for the rate of quenching of Cs($5D$) by ground-state perturbers. The role of out-of-multiplet quenching is discussed at length, and we have demonstrated that quenching by ground-state atoms dominates over that by cesium dimers under these conditions. In the pulsed-laser experiments, the temporal evolution of the $5D_J\rightarrow 6S$ and cascade $6P_{J'}\rightarrow 6S$ fluorescence was observed following either direct forbidden-line pumping of one fine-structure level, or indirect excitation of both fine-structure levels (i.e., molecular excitation followed by predissociation). Analysis of the buildup and decay rates of the various levels as a function of cesium density yields values for the natural lifetimes of the Cs($5D_J$) levels, as well as for the excitation transfer and quenching rates. Best values for the lifetimes and cross sections for Cs-Cs collisions obtained from these combined experiments are $\tau_{5D}=1250\pm115$ ns, $\sigma_{5/2\rightarrow 3/2}=36\pm8$ Å^2, and $\sigma_{5D}=30\pm3$ Å^2. In addition, numbers for the $6P$ level-quenching cross sections due to collisions with Cs atoms and Cs_2 molecules, respectively, were obtained: $\sigma_{6P}(\mathrm{Cs})=6.6\pm3.0$ Å^2 and $\sigma_{6P}(\mathrm{Cs_2})=863\pm260$ Å^2. In the discussion, we show how these new values can be used to reconcile the seemingly discrepant results of several previous studies.

PACS number(s): 34.50.Fa

I. INTRODUCTION

Investigations of collisional energy transfer in excited atomic and molecular states are of fundamental importance for a detailed understanding of inelastic or reactive collisions. Measurements of effective lifetimes and their dependence on pressure represent an accurate method for the determination of *absolute* cross sections of inelastic collisions in excited electronic states. An independent, steady-state method for measurements of collision cross sections is based upon studies of sensitized fluorescence. A comparison of the results from these two techniques allows a more reliable determination of systematic errors caused by radiation-trapping, line-broadening, and quenching effects. The present paper reports on such measurements of lifetimes and collisional deactivation of the Cs($5D_J$) levels, and compares the results of the two techniques.

Collisional transfer from one alkali-metal-atom fine-structure level to another (often called fine-structure mixing) has been studied extensively over the past 35 years. (See Refs. [1–16] for a selection of the more recent literature in this field. Reference [17] provides a complete review of the literature until 1975.) Such processes can be described by

$$A(n,l)_J+X\rightarrow A(n,l)_{J'}+X\ , \qquad (1)$$

where A represents the alkali-metal atom, and X is the collision partner (which may be a ground-state atom of the same species, a noble-gas atom, or another type of foreign-gas atom or molecule). Processes such as these are among the simplest forms of collisional excitation transfer and are therefore an important testing ground for theory.

One of the best studied sequences of collisional transfer among fine-structure levels involves the cesium nD_J states and ground-state-cesium perturbers:

$$\mathrm{Cs}(nD_{5/2})+\mathrm{Cs}(6S_{1/2})\rightleftharpoons\mathrm{Cs}(nD_{3/2})+\mathrm{Cs}(6S_{1/2})\ . \qquad (2)$$

Process (2) for $n=6-13$ has been studied by Tam *et al.* [1] and Sirko and Rosiński [8]. It has been found that, for these Rydberg levels, the mixing cross sections are basically geometric. In previous work, several authors have attempted to complete this sequence of measurements on the low end by studying mixing among the $5D_J$ levels [11,18]. However, such measurements are difficult due to the long wavelengths required for both the pumping and the detection.

The first estimate of the cross section for process (2) with $n=5$ was made by Wu and Huennekens [19], who pumped Cs_2 molecules with blue and green lines from an argon-ion laser and observed emission from atomic states populated by collisions and/or predissociation. The $5D_J$

levels were detected by observation of the weak $5D_J \rightarrow 6S_{1/2}$ dipole-forbidden but electric-quadrupole-allowed emission. In this work, it was found that the $5D_{5/2}$ to $5D_{3/2}$ state population ratio was approximately equal to 2 and independent of cesium density in the studied range $8\times10^{15} \leq [\mathrm{Cs}] \leq 1.4\times10^{17}$ cm^{-3} (where [Cs] represents the cesium atomic density). Since the complete mixing ratio in thermal equilibrium is $(g_2/g_1)\exp(-\Delta E/kT) \approx 1.1$ (which was observed in an identical cell under the same conditions but with $\frac{1}{2}$ atmosphere of neon buffer gas added), this implied either a very small mixing cross section (<2 Å^2) or an inexplicably large cesium atomic- or molecular-quenching rate. These measurements were consistent with an earlier experiment of McClintock and Balling [20], who measured a $5D_{5/2} \rightarrow 6S_{1/2}$ to $5D_{3/2} \rightarrow 6S_{1/2}$ forbidden-transition line-intensity ratio of 2.26 when exciting cesium vapor at a density of $\sim 2.5\times10^{16}$ cm^{-3} with 488-nm cw radiation.

Davanloo *et al.* [18] obtained the first quantitative determination of the $5D_J$ mixing cross section. Their experiment also involved pumping the Cs_2 molecule with visible light. However, they used a pulsed dye laser and probed the resulting excited-state atoms with a second delayed pulsed dye laser. They obtained the value $\sigma_{5/2\rightarrow3/2} = 17\pm10$ Å^2 for the process $\mathrm{Cs}(5D_{5/2}) + \mathrm{Cs}(6S) \rightarrow \mathrm{Cs}(5D_{3/2}) + \mathrm{Cs}(6S)$. However, to fit their data they needed to include a quenching term which they implied was of the form

$$\mathrm{Cs}(5D_J) + \mathrm{Cs}(6S) \rightarrow \mathrm{Cs}(6P, 6S) + \mathrm{Cs}(6S) \ . \qquad (3)$$

Since densities were not varied in their study, Davanloo *et al.* could only report a total $5D$ state collisional quenching rate of 4.7×10^5 s^{-1} at their Cs density of 2.6×10^{15} cm^{-3}. If it is assumed that process (3) is responsible for the quenching, then the cross section derived from these results is 46 ± 10 Å^2, almost three times greater than the Davanloo mixing cross section of 17 Å^2. This was surprising given that the $5D_J$ levels are separated by only 100 cm^{-1}, while the separation between $5D$ and $6P$ is almost 3000 cm^{-1}.

More recently, Keramati, Masters, and Huennekens [11] carried out a somewhat more direct measurement of the $5D_J$ mixing rate [process (2)]. These authors directly excited the dipole-forbidden but electric-quadrupole-allowed transition $6S_{1/2} \rightarrow 5D_{5/2}$ using a cw dye laser, and monitored the cascade $6P_J \rightarrow 6S_{1/2}$ fluorescence in the near infrared. Since $5D_{5/2}$ radiates exclusively to $6P_{3/2}$, only $6P_{3/2} \rightarrow 6S$ fluorescence is observed in the absence of collisional mixing. As the cesium density is increased, an increasing amount of $6P_{1/2} \rightarrow 6S$ fluorescence is observed. However, the $6P_{1/2}$ population can result from mixing that occurs in either the $5D$ or the $6P$ manifold. To discriminate between these two channels, a second set of measurements was carried out, under the same conditions, and essentially simultaneously, in which $6P_{3/2}$ was pumped directly from the ground state using a cw diode laser. This allowed the contribution from $6P_J$ fine-structure mixing to be effectively subtracted out, and a $5D_J$ mixing cross section of 70 ± 28 Å^2 was obtained. In this work, it was assumed that quenching due to process (3) was negligible since it requires conversion of almost 3000 cm^{-1} of internal energy into kinetic energy. Instead, these authors assumed that the dominant quenching mechanism would be

$$\mathrm{Cs}(5D_J) + \mathrm{Cs}_2(X\,^1\Sigma_g^+) \rightarrow \mathrm{Cs}(6P, 6S) + \mathrm{Cs}_2^* \ , \qquad (4)$$

where $\mathrm{Cs}_2(X\,^1\Sigma_g^+)$ and Cs_2^* represent ground- and electronically-excited-state cesium molecules, respectively. Process (4) is expected to have a large cross section (in sodium, cross sections for similar processes have been measured [21] to be ~ 370 Å^2) since the multitude of rovibrational levels in each electronic state creates a high probability for near-resonant energy transfer. However, because no electronic states lie 3000 cm^{-1} above the ground state, it is most likely that process (4) would lead primarily to the Cs($6S$) product. Under the conditions of Ref. [11] ($[\mathrm{Cs}_2] < 10^{13}$ cm^{-3}) process (4) was also considered to be negligible.

Because of the apparent discrepancies between the results of these previous experiments, we decided to carry out a complete set of measurements to determine the Cs($5D_J$) fine-structure-mixing cross section and to carefully investigate the role of quenching. We report here the results of both cw and pulsed laser studies of these processes. Our results generally confirm those of Davanloo *et al.* [18], although there is some quantitative disagreement. With these results it is now also possible to reconcile the seemingly contradictory results of all previous experiments.

This paper is organized as follows. In Sec. II, we present the rate equations and their solutions which were used in the analysis of both the pulsed and cw laser experiments. Section III describes both experimental setups. Section IV gives our results and compares them with those of previous works. Finally, Sec. V presents our conclusions.

II. RATE EQUATIONS

Figure 1 shows a cesium energy-level diagram with arrows representing all processes which were considered in the present work. In the five-state model, we have labeled $5D_{5/2}$, $5D_{3/2}$, $6P_{3/2}$, $6P_{1/2}$, and $6S_{1/2}$ as states 4, 3, 2, 1, and 0, respectively. Γ's are radiative rates while R's represent fine-structure mixing. Q's are quenching rates. It can be seen that separate rates have been included for quenching of the $5D_J$ levels to both $6P_{J'}$ levels and to $6S$. The $6P$ levels can only quench to $6S$. No excitation transfer into higher manifolds of states is considered since this would require conversion of $\geq 7kT$ of kinetic energy into internal energy.

A. cw experiment

In the cw experiment carried out here, the $5D_{5/2}$ level was pumped directly from the ground state on the dipole-forbidden but electric-quadrupole-allowed $6S_{1/2} \rightarrow 5D_{5/2}$ transition. The steady-state rate equation for the $5D_{3/2}$ density (n_3) is therefore given by

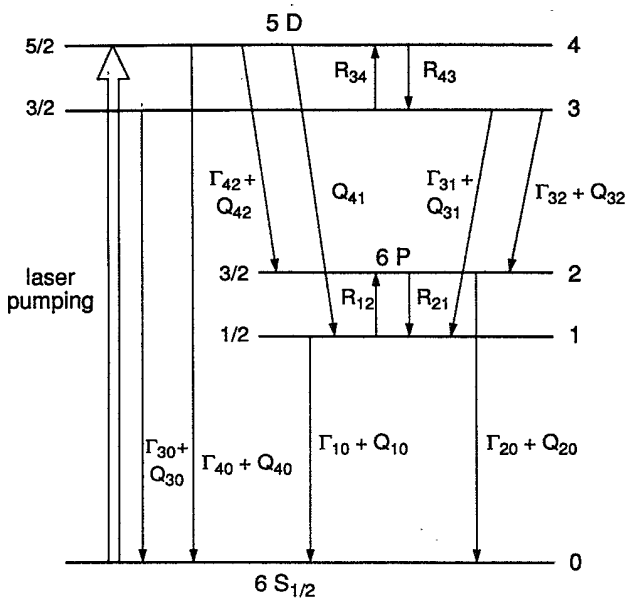

FIG. 1. Partial energy-level diagram of cesium (relative energies not to scale) showing collisional and radiative processes investigated in the present work. R's represent fine-structure mixing rates, Q's are quenching rates, and Γ's are radiative rates.

$$\dot{n}_3=0=R_{43}n_4-(\Gamma_{30}+\Gamma_{31}+\Gamma_{32}+Q_{30}+Q_{31}+Q_{32}+R_{34})n_3$$
$$=R_{43}n_4-(\Gamma_3+Q_3+R_{34})n_3\ , \tag{5}$$

where $\Gamma_3\equiv\Gamma_{30}+\Gamma_{31}+\Gamma_{32}$ and $Q_3\equiv Q_{30}+Q_{31}+Q_{32}$.

The experimentally measured quantity is the fluorescence ratio I_{31}/I_{42} which is related to the population ratio found from Eq. (5):

$$\frac{I_{31}}{I_{42}}=\frac{h\nu_{31}}{h\nu_{42}}\frac{\epsilon_{31}}{\epsilon_{42}}\frac{\Gamma_{31}}{\Gamma_{42}}\frac{n_3}{n_4}=\frac{\lambda_{42}}{\lambda_{31}}\frac{\epsilon_{31}}{\epsilon_{42}}\frac{\Gamma_{31}}{\Gamma_{42}}\frac{R_{43}}{(\Gamma_3+Q_3+R_{34})}\ . \tag{6}$$

Here, the ϵ's are the detection system efficiencies at the two wavelengths ($\lambda_{31}=3.01$ μm and $\lambda_{42}=3.49$ μm). $R_{34}/R_{43}=(g_4/g_3)\exp[-(E_4-E_3)/kT]\equiv\alpha$ from the principle of detailed balance. At low densities, the fluorescence ratio will scale linearly with density ($R_{43}=k_{43}[\mathrm{Cs}]$ where k_{43} is the rate coefficient for process (2)). At higher densities the fluorescence ratio versus density curve will saturate due to Q_3+R_{34} in the denominator. If either $Q\ll R$ or the quenching is atomic [process (3)], then the fluorescence ratio will reach a constant value at high density. If the quenching is molecular [process (4)], then the curve will eventually turn over, since the molecular density grows faster than the atomic density.

For completeness, we include the rate equations for the $6P_{1/2}$ and $6P_{3/2}$ states and for the $6P_{1/2}\rightarrow 6S$ to $6P_{3/2}\rightarrow 6S$ fluorescence ratio under these same pumping conditions:

$$\dot{n}_2=0=(\Gamma_{42}+Q_{42})n_4+(\Gamma_{32}+Q_{32})n_3+R_{12}n_1-(\Gamma_{20}+Q_{20}+R_{21})n_2\ , \tag{7a}$$

$$\dot{n}_1=0=Q_{41}n_4+(\Gamma_{31}+Q_{31})n_3+R_{21}n_2-(\Gamma_{10}+Q_{10}+R_{12})n_1\ , \tag{7b}$$

and

$$\frac{I_{10}}{I_{20}}=\frac{h\nu_{10}}{h\nu_{20}}\frac{\epsilon_{10}}{\epsilon_{20}}\frac{\Gamma_{10}}{\Gamma_{20}}\frac{n_1}{n_2}=\frac{\lambda_{20}}{\lambda_{10}}\frac{\epsilon_{10}}{\epsilon_{20}}\frac{\Gamma_{10}}{\Gamma_{20}}\frac{A}{B} \tag{8}$$

with

$$A\equiv R_{43}(\Gamma_{31}+Q_{31})(\Gamma_{20}+Q_{20}+R_{21})+R_{43}R_{21}(\Gamma_{32}+Q_{32})+R_{21}(\Gamma_{42}+Q_{42})(\Gamma_3+Q_3+R_{34})$$
$$+Q_{41}(\Gamma_{20}+Q_{20}+R_{21})(\Gamma_3+Q_3+R_{34})\ , \tag{8a}$$

and

$$B\equiv(\Gamma_{10}+Q_{10}+R_{12})[R_{43}(\Gamma_{32}+Q_{32})+(\Gamma_{42}+Q_{42})(\Gamma_3+Q_3+R_{34})]+R_{12}R_{43}(\Gamma_{31}+Q_{31})$$
$$+R_{12}Q_{41}(\Gamma_3+Q_3+R_{34})\ . \tag{8b}$$

These equations are analogous to Eqs. (3)–(5) of Ref. [11] which have been modified here to include the more general treatment of the quenching terms. Note that the resonance fluorescence will be strongly affected by radiation trapping under the conditions of these experiments. Therefore Γ_{10} and Γ_{20} must be treated as effective radiative rates (see Refs. [11] and [22]), which in general will vary with density.

B. Pulsed experiment

In the pulsed experiment, information about mixing and quenching rates is obtained more directly from the time dependence of the various excited-state populations which are monitored by the fluorescence. Since the duration of the laser pulses used in this experiment was less than 500 ps, the excitation can be considered to be a δ function in time, and the following rate equations are valid after the end of the laser pulse:

$$\dot{n}_4 = R_{34} n_3 - (\Gamma_4 + Q_4 + R_{43}) n_4 \ , \tag{9a}$$

$$\dot{n}_3 = R_{43} n_4 - (\Gamma_3 + Q_3 + R_{34}) n_3 \ , \tag{9b}$$

$$\dot{n}_2 = (\Gamma_{42} + Q_{42}) n_4 + (\Gamma_{32} + Q_{32}) n_3 + R_{12} n_1 - (\Gamma_{20} + Q_{20} + R_{21}) n_2 \ , \tag{9c}$$

$$\dot{n}_1 = Q_{41} n_4 + (\Gamma_{31} + Q_{31}) n_3 + R_{21} n_2 - (\Gamma_{10} + Q_{10} + R_{12}) n_1 \ , \tag{9d}$$

with $\Gamma_4 \equiv \Gamma_{40} + \Gamma_{42}$ and $Q_4 \equiv Q_{40} + Q_{41} + Q_{42}$. (Here we have neglected energy pooling and other excited-atom–excited-atom collision processes since the number of excited atoms produced by the weak pulsed laser is quite small.)

Equations (9a) and (9b) may be solved once the initial conditions are specified. In general, we find

$$n_4(t) = \frac{n_4(0)}{(\omega_+ - \omega_-)} \times [(\omega_+ - \Gamma_4 - Q_4 - R_{43}) \exp(-\omega_- t) - (\omega_- - \Gamma_4 - Q_4 - R_{43}) \exp(-\omega_+ t)] + \frac{n_3(0) R_{34}}{(\omega_+ - \omega_-)} [\exp(-\omega_- t) - \exp(-\omega_+ t)] \tag{10a}$$

and

$$n_3(t) = \frac{n_3(0)}{(\omega_+ - \omega_-)} \times [(\omega_+ - \Gamma_3 - Q_3 - R_{34}) \exp(-\omega_- t) - (\omega_- - \Gamma_3 - Q_3 - R_{34}) \exp(-\omega_+ t)] + \frac{n_4(0) R_{43}}{(\omega_+ - \omega_-)} [\exp(-\omega_- t) - \exp(-\omega_+ t)] \ , \tag{10b}$$

with

$$\omega_\pm = \tfrac{1}{2}(\Gamma_3 + \Gamma_4 + Q_3 + Q_4 + R_{34} + R_{43}) \pm \tfrac{1}{2}[(\Gamma_3 - \Gamma_4 + Q_3 - Q_4 + R_{34} - R_{43})^2 + 4 R_{34} R_{43}]^{1/2} . \tag{11}$$

For the specific case of direct pumping of the $5D_{5/2}$ level on the quadrupole transition from the ground state, we set $n_3(0) = 0$ and obtain

$$n_4(t) = \frac{n_4(0)}{(\omega_+ - \omega_-)} [(\omega_+ - \Gamma_4 - Q_4 - R_{43}) \exp(-\omega_- t) - (\omega_- - \Gamma_4 - Q_4 - R_{43}) \exp(-\omega_+ t)] \tag{12a}$$

and

$$n_3(t) = \frac{n_4(0) R_{43}}{(\omega_+ - \omega_-)} [\exp(-\omega_- t) - \exp(-\omega_+ t)] \ . \tag{12b}$$

For pumping of the $5D_{3/2}$ state, Eqs. (12a) and (12b) remain valid if the subscripts 4 and 3 are simply interchanged.

When the $5D_J$ levels are populated by predissociation of the Cs_2 molecule, following excitation into the $E\,^1\Sigma_u^+$ state by the 488-nm Ar^+-laser line, the more general equations [(10a) and (10b)] must be used, with the appropriate initial condition [i.e., at the end of the laser pulse the ratio $n_3(0)/n_4(0) \sim 1.5$; see Ref. [23]].

Finally, we note that when either of the $5D_J$ levels is excited, the pulsed rate equations (9) may be solved for the $6P_{J'}$ level populations. These may be represented by the following:

$$n_{1,2} = A_{1,2} \exp(-\omega_- t) + B_{1,2} \exp(-\omega_+ t) + C_{1,2} \exp(-\lambda_- t) + D_{1,2} \exp(-\lambda_+ t) \ , \tag{13}$$

where

$$\lambda_\pm = \tfrac{1}{2}(\Gamma_{10} + \Gamma_{20} + Q_{10} + Q_{20} + R_{12} + R_{21}) \pm \tfrac{1}{2}[(\Gamma_{10} - \Gamma_{20} + Q_{10} - Q_{20} + R_{12} - R_{21})^2 + 4 R_{12} R_{21}]^{1/2} . \tag{14}$$

The amplitudes are, in general, quite complicated, and will not be reproduced here.

III. EXPERIMENT

A. cw experiment

The setup for the cw laser experiment is shown in Fig. 2. Pure cesium vapor was confined in a cross-shaped stainless-steel cell with sapphire windows which has been described in previous publications [24,25]. The cell, which is connected to a vacuum and gas-handling system through a series of valves, is heated by a set of cartridge heaters to a temperature which was fixed at 601 K throughout the measurements. The cesium density is controlled by the temperature of an independently heated reservoir located in a sidearm of the cell. Two sapphire rods, filling two arms of the cross, create a slab-shaped interaction region with a thickness of 0.55 cm. Cesium atomic densities were determined by the absorption equivalent width technique, using a white-light source.

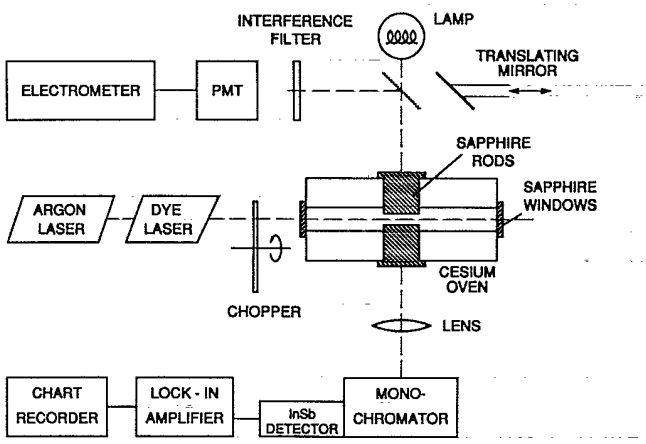

FIG. 2. Schematic diagram of the setup for the cw experiment. PMT is the photomultiplier tube.

Such absorption scans of the $6S_{1/2}\rightarrow 6P_{3/2}$ transition could be obtained in either pure cesium, or in cesium-argon mixtures. In either case, the equivalent width of the resonance transition is dominated by pressure broadening, and is given by [24]

$$W_\lambda = \frac{\lambda^2}{c}\left[\frac{\lambda^2}{8\pi^2}\frac{g_2}{g_1} L n \Gamma_c \Gamma_{\rm nat}\right]^{1/2} . \tag{15}$$

Here g_1 and g_2 are the statistical weights of the lower and upper states, respectively, λ is the transition wavelength, L is the absorption path length, n is the atom density, and $\Gamma_{\rm nat}$ is the natural radiative rate (Einstein A coefficient) of the transition. Γ_c, the collisional line-broadening rate, has a contribution from self-broadening, and if argon is present, one from foreign-gas broadening; i.e., $\Gamma_c = n_{\rm Cs} k_c^{\rm Cs-Cs} + n_{\rm Ar} k_c^{\rm Cs-Ar}$. The self-broadening constant is taken from Ref. [26] ($k_c^{\rm Cs-Cs} = 7.51\times 10^{-7}$ cm^3 s^{-1}). Theoretical self-broadening rates of Ref. [26] have been verified in the case of sodium [5] to within experimental uncertainties of $\pm 15\%$. $k_c^{\rm Cs-Ar} = 5.33\times 10^{-9}$ cm^3 s^{-1} from Ref. [27]. Cesium densities derived from the equivalent width technique are typically accurate to within approximately 10–15 %, but differ from those obtained from the Nesmeyanov vapor-pressure formula [28] by as much as a factor of 2 (see also Ref. [11]).

Cs_2 molecular densities can be obtained from the equilibrium constant $K_{\rm eq}(T) = [{\rm Cs}]^2/[{\rm Cs}_2]$, which in turn depends on the Cs_2 ground-state molecular constants [29]. Using the constants of Weickenmeier *et al.* [30], we obtain

$$K_{\rm eq}(T) = 1.37\times 10^{22} T^{0.5} \exp(-5.22\times 10^3/T) \times [1-\exp(-60.46/T)] \tag{16}$$

for T in K. At the fixed cell temperature of 601 K, we have $K_{\rm eq}(T=601\ {\rm K}) = 5.43\times 10^{18}$ cm^{-3}.

Cesium atoms in the vapor were excited using a multimode cw dye laser tuned to the $6S\rightarrow 5D_{5/2}$ electric quadrupole transition. Fluorescence was detected through the two faces of the slab-shaped interaction region in directions that were perpendicular to the laser propagation axis. In one direction, the total $6P_{3/2}\rightarrow 6S$ fluorescence was monitored using an S-1 photomultiplier and a Cs-D_2-line interference filter. In the other direction, fluorescence was directed into a 0.22-m monochromator with a 150-line/mm grating, and 3-mm slits (resulting in a spectral resolution of $\sim$90 nm, which was sufficient to separate the $5D_J\rightarrow 6P_{J'}$ fine-structure components). Light passing through the monochromator at $\lambda = 3.01$ and 3.49 μm, corresponding to the $5D_{3/2}\rightarrow 6P_{1/2}$ and $5D_{5/2}\rightarrow 6P_{3/2}$ transitions, respectively, was detected with a liquid-nitrogen-cooled InSb detector (Electro-Optical Systems). These signals were divided by the total $6P_{3/2}\rightarrow 6S$ fluorescence intensity, which was simultaneously monitored, in order to correct for minor drifts of the laser frequency. The laser beam was chopped and lock-in detection was used. Signals were recorded with a strip-chart recorder.

Calibration of the detection system at the two wavelengths was carried out by measuring the ratio I_{31}/I_{42} at low cesium density ($\sim 1\times 10^{15}$ cm^{-3}) but with a large pressure (100–300 Torr) of argon buffer gas. Under these conditions, collisions with the inert gas atoms cause much excitation transfer between the fine-structure levels but presumably no quenching. Thus Eq. (6) is valid with $R_{34} \gg \Gamma_3, Q_3$. Therefore we find

$$\left[\frac{I_{31}}{I_{42}}\right]_{\rm argon} = \frac{\lambda_{42}}{\lambda_{31}}\frac{\epsilon_{31}}{\epsilon_{42}}\frac{\Gamma_{31}}{\Gamma_{42}}\frac{R_{43}}{R_{34}} = \frac{\lambda_{42}}{\lambda_{31}}\frac{\epsilon_{31}}{\epsilon_{42}}\frac{\Gamma_{31}}{\Gamma_{42}}\alpha^{-1} \equiv N\alpha^{-1} , \tag{17}$$

where α is defined just below Eq. (6) and is equal to 1.19 at 601 K. The experimentally measured fluorescence ratio was found to increase with argon pressure, but saturated at a value of 1.15. (This same value was obtained at $P = 100$ and 259 Torr, thus verifying that the approximation $R_{34} \gg \Gamma_3, Q_3$ is valid.) Thus we find that $N = (\lambda_{42}/\lambda_{31})(\epsilon_{31}/\epsilon_{42})(\Gamma_{31}/\Gamma_{42}) = 1.15\times 1.19 = 1.37$ for our detection system.

A series of measurements of I_{31}/I_{42} was then carried out in pure cesium vapor for a range of densities between 1.1×10^{15} and 1.1×10^{16} cm^{-3}. Equation (6) was then fit to these values using the above calibration and taking $k_{43} \equiv R_{43}/[{\rm Cs}]$ and $q_3 \equiv Q_3/[{\rm Cs}]$ (or $q_3 \equiv Q_3/[{\rm Cs}_2] = Q_3 K_{\rm eq}/[{\rm Cs}]^2$ depending on the form of quenching [process (3) or (4)] which is assumed) as the fitting parameters. The results of this procedure are presented in Sec. IV.

B. Pulsed experiment

The experimental setup for the pulsed measurements is shown in Fig. 3. The cesium vapor was contained in a 2.3-cm-diam linear heat-pipe oven [31,32] in which the argon gas pressure was set to the cesium pressure calculated from the Nesmeyanov vapor pressure formula [28] for the relevant temperature. It was verified that this procedure resulted in true heat-pipe regime operation.

Thus the cesium pressure was simply equal to that of the buffer gas. The heat-pipe temperature was varied in the range 480 K $< T <$ 637 K, corresponding to a cesium atomic pressure ranging between 0.11 and 10 Torr.

The vapor was excited using a cavity-dumped, mode-locked-laser system which was used in two configurations. For direct excitation of the dipole-forbidden transition $6S_{1/2} \rightarrow 5D_J$ ($\lambda = 689.7$ and 685.1 nm for $J = \frac{3}{2}$ and $\frac{5}{2}$, respectively) ultrafast pulses were provided by a dye laser operating with DCM dye [4-(dicyanomethylene)-2-methyl-6-(*p*-dimethyl-aminostyryl)-4*H*-pyran], synchronously pumped by a mode-locked Ar^+ laser. A cavity-dumper system inserted in the dye-laser cavity allowed us to vary the repetition rate up to 4 MHz. The pulsewidth of 400 ps was monitored by a fast photodiode and a sampling oscilloscope. The laser wavelength was measured by means of a computer-controlled Fabry-Pérot wavemeter [33].

In the second configuration, the $5D_J$ levels were populated by exciting the Cs_2 molecule with the 488-nm Ar^+ laser line to levels (v',J') of the $E\,^1\Sigma_u^+$ state, which preferentially predissociates to the $5D_{3/2}$ level [23,34]. In this case the Ar^+ laser operated in the cw regime in an extended optical cavity by removing the output coupler mirror. A cavity-dumper system made up part of this extended cavity, providing laser pulses of about 20 ns in width. The larger pulsewidth compared to the mode-locking operation was, however, sufficiently short for our investigation because the effective lifetimes of the studied levels are in the microsecond range.

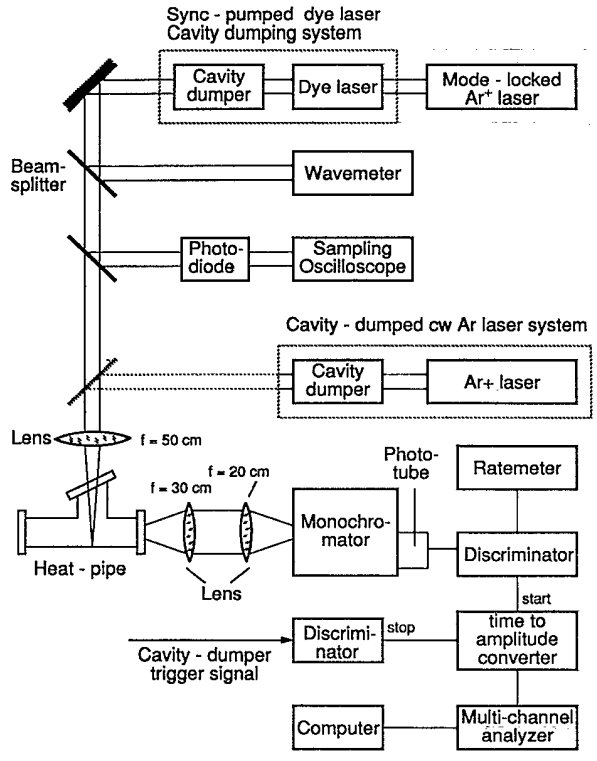

FIG. 3. Setup for the pulsed-laser experiment. Direct excitation of the Cs($5D_J$) levels was achieved using a synchronously pumped dye laser, while for the molecular excitation scheme an Ar^+ laser ($\lambda = 488$ nm) was operated in a cavity-dumped cw configuration. Fluorescence was time resolved by means of the delayed-coincidence technique.

The laser beam was focused in the middle of the heat pipe by means of a lens with 50-cm focal length. The fluorescence on the electric quadrupole $5D \rightarrow 6S$ and the cascade $6P \rightarrow 6S$ fluorescence was detected transverse to the laser-excitation axis. The fluorescence was collected on the entrance slit of a 1-m monochromator with a 1200-line/mm grating (10-Å/mm dispersion) and detected by means of a photomultiplier (RCA model C31034A). The slits were fully opened (3 mm) to improve the signal-to-noise ratio, especially for the forbidden $5D \rightarrow 6S$ fluorescence. Lifetime measurements with direct excitation of a $5D_J$ level and detection of its fluorescence were not possible because the resonance fluorescence was completely masked by the scattered laser light which saturated the photodetector. However, the sensitized fluorescence, originating from collisional excitation transfer from the other fine-structure level, could be spectrally separated and detected. The scattered light, which was still present on the sensitized fluorescence, could be easily discriminated due to the short pulsewidth of the laser. With the other scheme, based on molecular excitation with the 488-nm Ar^+-laser line, the scattered light was readily removed by inserting a cutoff filter in front of the heat-pipe window.

The time evolutions of the $5D$ and $6P$ levels were obtained by means of the delayed-coincidence technique [35]. The fluorescence photon starts a voltage ramp which is stopped by the laser trigger signal, and a time-to-amplitude converter provides a voltage signal that is stored in a multichannel analyzer. For both excitation schemes mentioned above the laser repetition rate was chosen as high as possible with respect to the studied decay rates. The counting time required to obtain good statistics on the fluorescence decay curves was shorter ($T \approx 30$ min) for the molecular excitation scheme than for the direct excitation of the quadrupole $6S \rightarrow 5D$ transition ($T \approx 60$ min), demonstrating the more efficient way of populating the $5D$ levels through the predissociation channel. Since typical count rates of approximately one count per 100 laser pulses were used, pileup effects were negligible.

Finally, the data were sent to a computer, allowing us to fit the decay curves with single- or multiexponential functions.

It should be noted that excited atomic levels were populated only weakly either by the molecular photodissociation or the forbidden atomic line pumping. The largest excited-atom densities were obtained using the photodissociation technique, and thus are certainly limited by the molecular density which is roughly two orders of magnitude smaller than the ground-state-atom density. In fact, since the pulsed laser used for this pumping was itself quite weak, and the photodissociation process is not 100% efficient, the actual excited-state densities were probably several orders of magnitude smaller than this limit. The low fluorescence-photon count rates obtained with wide-open monochromator slits attest to the small excited-atom populations. Thus, under these conditions,

excited-atom–excited-atom collision processes, such as energy pooling and associative ionization, can be completely neglected.

IV. RESULTS AND DISCUSSION

A. cw experiment

Figure 4 shows the results obtained in the cw experiment. Due to the fact that the laser was pumping a very weak dipole-forbidden transition, and that the monitored fluorescence occurred in the infrared where detectors are not very sensitive, the signal-to-noise ratio was not as high as one might like. The error bars on the experimental points in Fig. 4 are estimates which we believe cover the measurement uncertainty in the fluorescence ratios, as well as the uncertainty in the cesium density.

The data are fit by a function of the form of Eq. (6). If the dominant quenching term is atomic [process (3)], then the fitting function becomes

$$\frac{I_{31}}{I_{42}}=N\frac{k_{43}[\mathrm{Cs}]}{\Gamma_3+(q_3+\alpha k_{43})[\mathrm{Cs}]} . \quad (18)$$

On the other hand, if the dominant quenching term is molecular [process (4)], then the data must be fit by the function

$$\frac{I_{31}}{I_{42}}=N\frac{k_{43}[\mathrm{Cs}]}{\Gamma_3+\alpha k_{43}[\mathrm{Cs}]+q_3[\mathrm{Cs}_2]}$$
$$=N\frac{k_{43}[\mathrm{Cs}]}{\Gamma_3+\alpha k_{43}[\mathrm{Cs}]+(q_3/K_{\mathrm{eq}})[\mathrm{Cs}]^2} , \quad (19)$$

where in the last step we have used the fact that the cell temperature was kept constant in the experiment.

It can be seen that the function in Eq. (18) builds linearly with density at low densities and saturates at the value $N/[\alpha+(q_3/k_{43})]$ at high densities. If Eq. (19) is correct, then the data will build up linearly, saturate, and eventually turn over and decrease as the density is increased further. In either event, we know that the quenching term is important since the data are clearly saturating at a value that is much less than that which would be obtained in the absence of quenching, $N/\alpha=1.15$. However, the data in Fig. 4 do not cover a sufficiently large range of densities to distinguish between Eqs. (18) and (19) on their own. Higher densities than those reported in Fig. 4 could not be studied here since the silver O-ring window seals degrade under such conditions.

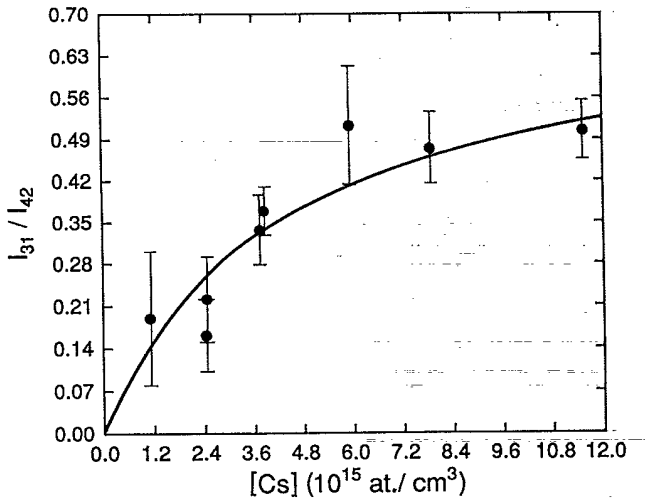

FIG. 4. Plot of I_{31}/I_{42} vs cesium density in the cw experiment. The solid line is the least-squares best fit of the data using two free parameters (k_{43} and q_3).

Nonetheless, we can conclude that the atomic quenching mechanism and Eq. (18) are correct for the full range of Cs_2 densities studied here by also considering the earlier results of Wu and Huennekens [19]. Those authors report $I_{30}/I_{40}=0.5$, independent of density for densities in excess of 10^{17} cm^{-3} following excitation of the Cs_2 molecule with an argon-ion laser. Adding $\frac{1}{2}$ atmosphere of neon resulted in $I_{30}/I_{40}=0.91$. Since $[\mathrm{Cs}_2]/[\mathrm{Cs}]$ was more than a factor of 5 greater in that earlier work than in the present experiments, it is clear that these results are inconsistent if the quenching is molecular, but are completely compatible if the quenching is atomic. (In particular, fitting the current data with a molecular-quenching term yields $q_3=3.6\times10^{-8}$ cm^{3}s^{-1}. With this value, I_{30}/I_{40} should have dropped to ~0.2 at $[\mathrm{Cs}]=10^{17}$ cm^{-3} in the Wu and Huennekens experiment if the quenching is molecular.) This conclusion is also verified by the more-accurate pulsed-laser data presented in Sec. IV B, which allow direct observation of the quenching, and show that it is linear in atomic number density.

Based upon this discussion, we fit the data of Fig. 4 with Eq. (18) in a weighted least-squares procedure. From this fit, we obtain the following values for the mixing and quenching rate coefficients:

$$k_{43}=(1.36^{+0.47}_{-0.39})\times10^{-10}\ \mathrm{cm}^3\mathrm{s}^{-1} \quad (20)$$

and

$$q_3=(1.0^{+0.8}_{-0.6})\times10^{-10}\ \mathrm{cm}^3\mathrm{s}^{-1} . \quad (21)$$

In the fit, we used a theoretical value [36] $\Gamma_3=1.17\times10^6$ s^{-1}, as was done in Ref. [11]. Because in the pulsed-laser experiment (see Sec. IV B) we measured $\Gamma_{5D}=\tau_{5D}^{-1}=8.0\times10^5$ s^{-1} (where τ_{5D} is the average lifetime of the $5D_J$ levels in the absence of collisions), we assume that this number is only accurate to $\sim20\%$. This uncertainty in Γ_3 and possible systematic errors in [Cs] are the main contributors to the error limits in Eqs. (20) and (21).

In this fit, the parameter q_3 is not determined nearly as well as k_{43} since the two parameters are partially correlated and since the density range of the data was not very large. However, we note that Wu and Huennekens's result can be added to the present data field to improve the fit. Their result for the $5D_J\rightarrow6S$ forbidden-line-intensity ratio translates into a value of

$$I_{31}/I_{42}=(N/N')(I_{30}/I_{40})$$
$$=N[\alpha(I_{30}/I_{40})_{\mathrm{neon}}]^{-1}(I_{30}/I_{40})=0.68 .$$

This is in good agreement with the saturation limit of 0.71 predicted from the present results [(20) and (21)] and Eq. (18). Including this point in our fit, the mixing and quenching rates are hardly affected [$k_{43}=(1.42\pm0.39)\times10^{-10}$ cm^3 s^{-1} and $q_3=(1.14^{+0.56}_{-0.44})\times10^{-10}$ cm^3 s^{-1}], but the uncertainty in the quenching is reduced considerably.

If we assume that the cross sections are independent of velocity, we may define an average cross section by

$$k=\langle\sigma v\rangle\approx\sigma\bar{v}\ , \tag{22}$$

where $\bar{v}=[8RT(M_1+M_2)/\pi M_1M_2]^{1/2}$ is the mean relative velocity of the two colliding atoms. Under our conditions, $T=601$ K, we find $\bar{v}=4.36\times10^4$ cm/s and therefore the combined cw measurements result in

$$\sigma_{43}=33\pm9\ \text{Å}^2 \tag{23}$$

and

$$\sigma_3=26\pm12\ \text{Å}^2 \tag{24}$$

for the mixing and out-of-multiplet-quenching cross sections.

B. Pulsed experiment

In the pulsed experiment, the $5D_J$ levels could be populated either directly using the dye laser (tuned to the $6S\rightarrow5D_J$ electric-quadrupole transition frequencies) or by predissociation following pumping of the E states of the Cs_2 molecule using the mode-locked argon-ion laser at $\lambda=488$ nm. While the former excitation scheme was needed to prepare a single $5D_J$ level, and therefore necessary to obtain information on the fine-structure mixing rate, the latter scheme resulted in much better signal-to-noise ratios and proved more useful in obtaining the natural lifetimes and quenching rates.

Typical time-resolved fluorescence signals of the $5D_{3/2}\rightarrow6S_{1/2}$ transition are shown in Fig. 5 at two different temperatures. The $5D_{3/2}$ level was populated by fine-structure collisional mixing following direct excitation of the $5D_{5/2}$ level.

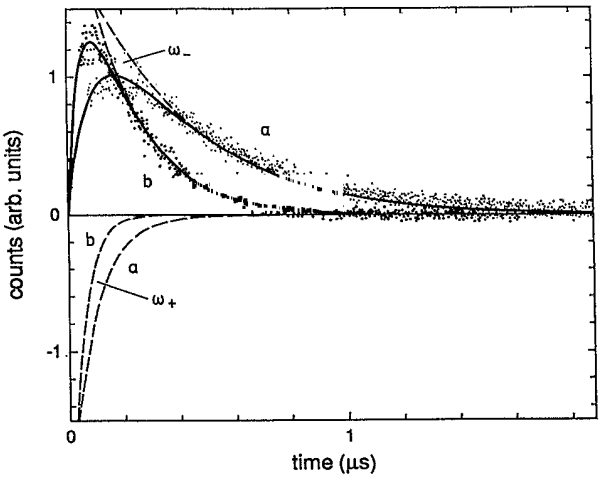

FIG. 5. Time-resolved fluorescence of the quadrupole-allowed cesium $5D_{3/2}\rightarrow6S_{1/2}$ transition ($\lambda=689.7$ nm) at (a) $T=257$ °C and (b) $T=287$ °C, following direct laser pumping of the $5D_{5/2}$ state from the $6S_{1/2}$ ground state. The solid curves are the best fit of the data using Eq. (12b), while the two exponentials with decay constants ω_+ and ω_- are represented by dashed lines.

Regardless of pumping scheme, the $5D_J\rightarrow6S$ fluorescence can be described as a sum of two exponentials with decay constants given by Eq. (11). For direct $5D_J$ level pumping using the dye laser, we obtain ω_+ from the buildup rate and ω_- from the late time decay of the transferred component (sensitized fluorescence component). The directly pumped component cannot be used because the photodetector becomes saturated with scattered laser light.

For relatively high densities where $\Gamma_3-\Gamma_4\ll R_{34}-R_{43}$, Eq. (11) cannot be easily approximated, since we do not know the magnitude of Q_3-Q_4. However, if we assume that $Q_3=Q_4\equiv Q_D$, then Eq. (11) can be approximated in this limit as

$$\begin{aligned}\omega_\pm\approx s_\pm&\equiv\frac{\Gamma_3+\Gamma_4}{2}\pm\frac{(\alpha-1)}{(\alpha+1)}\frac{\Gamma_3-\Gamma_4}{2}+Q_D+\frac{(\alpha+1)R_{43}\pm(\alpha+1)R_{43}}{2}\\&=\frac{\Gamma_3+\Gamma_4}{2}\pm\frac{(\alpha-1)}{(\alpha+1)}\frac{\Gamma_3-\Gamma_4}{2}+\left[\sigma_{5D}+\frac{(\alpha+1)\sigma_{43}\pm(\alpha+1)\sigma_{43}}{2}\right][\text{Cs}]\bar{v}\ .\end{aligned} \tag{25}$$

[In the high density limit, the first two terms on the right-hand side of Eq. (25) are small compared to the density-dependent terms. However, they will be needed later for the extrapolations of $s_\pm$ to zero density. The approximation given here for the density-dependent term is equivalent to the approximation that $Q_3-Q_4\ll R_{34}+R_{43}$. The latter inequality is probably satisfied by roughly a factor of 10 at all densities.]

The dependences of s_+ and s_- on $[\text{Cs}]\bar{v}$ yield typical Stern-Volmer plots whose slopes give

$$\sigma_{5D}\ \ (\text{from } s_-) \tag{26a}$$

and

$$\sigma_{5D}+(\alpha+1)\sigma_{43}\ \ (\text{from } s_+)\ . \tag{26b}$$

Values of ω_+ and ω_- obtained by fitting the time dependence of the sensitized $5D_{3/2}\rightarrow6S_{1/2}$ fluorescence are plotted in Fig. 6 versus $[\text{Cs}]\bar{v}$. We have verified that the sensitized fluorescence decay rates $\omega_\pm$ obtained from the direct excitation of both $5D_J$ fine-structure levels are con-

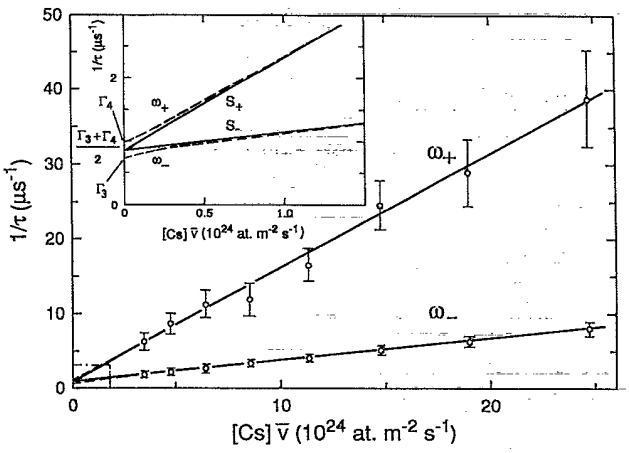

FIG. 6. Stern-Volmer plots of the exponential factors ω_+ and ω_- describing the decay of the $5D_{3/2}$ level after direct excitation of the $5D_{5/2}$ level (open points). Solid lines are the result of a best fit using Eq. (25) as explained in the text. The solid lines represent the approximate solutions $s_\pm$, while the dashed lines represent the exact solutions $\omega_\pm$ from Eq. (11). For the latter curves Γ_3 and Γ_4 have been taken from Ref. [45]. In the inset, the region of low cesium density is magnified.

sistent.

From the slope of s_-, we obtain the quenching cross section

$$\sigma_{5D}=30\pm5\ \text{Å}^2\ . \tag{27}$$

It can be seen that this quenching rate agrees with that obtained in the cw experiment, but is determined with higher accuracy.

From the sensitized fluorescence buildup rate ω_+ it is also possible to estimate the fine-structure mixing rate. Indeed, from the slope of s_+ and using Eq. (26), we obtain

$$\sigma_{43}=55\pm25\ \text{Å}^2\ . \tag{28}$$

The larger error limits here reflect the higher uncertainty in the determination of ω_+ compared to ω_- from the time-dependent fluorescence signals shown in Fig. 5. In this case, the agreement between the pulsed and cw results is not quite as good as for the quenching cross section, but is still within combined error bars. For our conditions, the mixing rate is more accurately determined from the cw measurements.

The straight-line extrapolations to zero density of s_+ and s_- yield weighted averages of the $5D_J$ fine-structure-level radiative rates $[(\alpha\Gamma_3+\Gamma_4)/(\alpha+1)$ for s_+ and $(\Gamma_3+\alpha\Gamma_4)/(\alpha+1)$ for $s_-]$. In principle, one could determine both Γ_3 and Γ_4 independently from the two intercepts of s_+ and s_-. For instance, the sum of the intercepts yields $\Gamma_3+\Gamma_4$, and their difference yields $(\alpha-1)(\Gamma_3-\Gamma_4)/(\alpha+1)$. However, since α is close to 1 under our conditions, and $\Gamma_3\sim\Gamma_4$, both intercepts are very close to the average radiative rate $(\Gamma_3+\Gamma_4)/2$. In fact, the experimental uncertainties of these intercepts is larger than their difference, so it is only meaningful to report an average effective radiative rate; i.e., we assume $\Gamma_3\sim\Gamma_4\equiv\Gamma_{5D}$ and calculate an effective radiative lifetime from each intercept according to $\tau_{5D}=\Gamma_{5D}^{-1}$. In this manner we obtain

$$\tau_{5D}=1295\pm200\ \text{ns}\ \ (\text{from } s_-) \tag{29a}$$

and

$$\tau_{5D}=1059\pm400\ \text{ns}\ \ (\text{from } s_+)\ . \tag{29b}$$

The error limits on the determination of the average lifetime from s_+ are larger due to the greater uncertainty in determining the buildup rate from the data (see Fig. 6).

In the limit of very low density, each $5D$ level simply decays with its own radiative decay rate $\Gamma_J=\tau_J^{-1}$. The zero-density intercept of the actual measured decay rates $\omega_\pm$ (as opposed to the extrapolated high-density decay rates $s_\pm$) versus $[\text{Cs}]\bar{v}$ would therefore yield the inverses of the natural lifetimes individually. This is shown in the inset of Fig. 6. Nevertheless, $\omega_\pm$ differ significantly from $s_\pm$ only at densities that are so low as to make the photon-counting acquisition time prohibitively long, and consequently we did not attempt this.

When using the molecular-predissociation pumping scheme, the $5D$ levels are more effectively populated than in the case of direct forbidden-line atomic excitation. Moreover, in this scheme, both $5D$ levels are populated and the general expressions (10) must be used. Under these conditions, the ω_+ exponentials become less important, and each $5D_J$ level fluorescence signal is well fitted by a single exponential decay. However, for the lowest cesium density studied in our experiment, collisional mixing is still rapid compared to the radiative lifetime and, as a consequence, both levels decay with the same rate ω_-. The average of the two fine-structure decay rates is shown in Fig. 7. The extrapolation to zero density yields the weighted average of the natural radiative rates of the

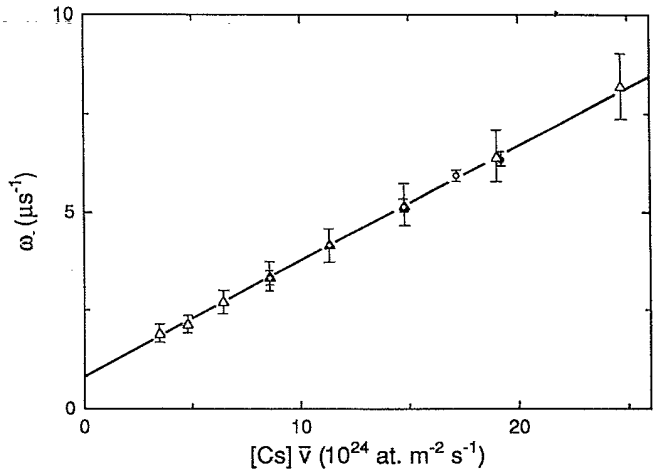

FIG. 7. Dependence of the weighted average inverse effective lifetimes of the $5D_{3/2}$ and $5D_{5/2}$ levels populated through E-state excitation of Cs_2 followed by predissociation (points with smaller error bars). The triangles (with larger error bars) result from the direct excitation scheme. (These latter points are the data already depicted in the lower curve of Fig. 6.)

TABLE I. Lifetimes and radiative decay rates of the Cs($5D_J$) levels.

Ref.	$\Gamma_{5D_{3/2}\rightarrow 6P_{1/2}}$ (s^{-1})	$\Gamma_{5D_{3/2}\rightarrow 6P_{3/2}}$ (s^{-1})	$\tau_{5D_{3/2}}=(\Gamma_{5D_{3/2}\rightarrow 6P_{1/2}}+\Gamma_{5D_{3/2}\rightarrow 6P_{3/2}})^{-1}$ (ns)	$\Gamma_{5D_{5/2}\rightarrow 6P_{3/2}}$ (s^{-1})	$\tau_{5D_{5/2}}=(\Gamma_{5D_{5/2}\rightarrow 6P_{3/2}})^{-1}$ (ns)
Theory					
Warner [36]	10.5×10^5	1.22×10^5	855.6	8.40×10^5	1190
Fabry [42]	8.42×10^5	0.99×10^5	1062	6.97×10^5	1435
Stone [43]	9.23×10^5	1.08×10^5	970.3	7.45×10^5	1342
Heavens [44]	9.4×10^5	1.1×10^5	952	7.30×10^5	1370
Theodosiou [45]			908.7	7.80×10^5	1282
Experiment					
This work[a]			1250±115		1250±115
Marek [46][b]			890±90		890±90

[a]Average lifetime of the $5D_J$ levels. Individual lifetimes could not be obtained because of fine-structure mixing at the lowest densities studied.
[b]Average lifetime of the $5D_J$ levels. Individual lifetimes could not be obtained because of fine-structure mixing occurring in collisions with xenon buffer-gas atoms.

two $5D_J$ fine-structure levels, while the slope provides the quenching cross section. In this manner we obtain

$$\tau_{5D}=1250\pm150 \text{ ns} \tag{30}$$

and

$$\sigma_{5D}=30\pm3 \text{ Å}^2 . \tag{31}$$

These values are in agreement with those obtained from the direct atomic-excitation scheme, but are determined with higher accuracy.

Our results for the $5D$ state lifetimes are compared to previous theoretical and experimental values in Table I. Our mixing and quenching rates are presented in Table II, where they are also compared to the results of previous measurements.

It is also useful to look at the $6P\rightarrow6S$ cascade fluorescence in the pulsed experiment to see what it can tell us. In general, the solutions for the $6P_{J'}$ level populations when pumping one of the $5D_J$ levels [Eqs. (13) and (14)] are too complicated to provide much insight. However, if we consider the simpler three-level model shown in Fig. 8, which ignores the fine-structure splittings, we obtain

$$\dot{n}_D=-(\Gamma_{DP}+\Gamma_{DS}+Q_{DP}+Q_{DS})=-(\Gamma_D+Q_D)n_D \tag{32a}$$

and

$$\dot{n}_P=(\Gamma_{DP}+Q_{DP})n_D-(\Gamma_P+Q_P)n_P , \tag{32b}$$

with the solutions

$$n_D(t)=n_D(0)\exp[-(\Gamma_D+Q_D)t] \tag{33a}$$

and

$$n_P(t)=\frac{(\Gamma_{DP}+Q_{DP})n_D(0)}{(\Gamma_D+Q_D-\Gamma_P-Q_P)}\times\{\exp[-(\Gamma_P+Q_P)t]-\exp[-(\Gamma_D+Q_D)t]\} . \tag{33b}$$

In this simplified model, it can be seen that the $6P$ population will build up with the faster and decay with the slower of the two rates (Γ_D+Q_D) and (Γ_P+Q_P). Since the observed $6P$ fluorescence decays much more slowly than the $5D$ fluorescence, it is clear that (Γ_P+Q_P) is the slower rate. Thus the $6P$ fluorescence buildup rate roughly gives Γ_D+Q_D, while the slow decay rate gives Γ_P+Q_P. The $6P\rightarrow6S$ fluorescence is highly trapped [37,38]. However, in the density range studied, the trapping is dominated by the self-broadened line wings, and Γ_P is roughly constant [22]. Thus plots of the slower $6P$ level decay rate versus atomic or molecular cesium densities provide information on the quenching mechanisms and trapped lifetimes.

In our pulsed experiment, we have recorded both the D_1 and D_2 resonance fluorescence, but a systematic analysis was made only for the $6P_{3/2}\rightarrow6S_{1/2}$ cascade

TABLE II. Cs($5D_J$) fine-structure mixing and quenching cross sections.

Reference	$\sigma_{5/2\rightarrow3/2}$ (Å^2)	σ_{5D} (Å^2)
Wu and Huennekens [19][a]	<2	
Davanloo *et al.* [18]	17±10	46±10
Keramati, Masters, and Huennekens [11][b]	70±28	
This work		
pulsed	55±25	30±3
cw	33±9	26±12
best values	36±8	30±3
Geometric[c]	14	

[a]This result can now be discarded since it was based upon an assumption that no quenching occurred (see text).
[b]This result is approximately a factor of 2 too large due to neglect of atomic quenching (see text).
[c]The geometric cross section was approximated by the hydrogenic expectation value of the square of the orbit radius given by [47] $r^2=\frac{1}{2}n^{*2}[5n^{*2}+1-3l(l+1)]a_0^2$, where $n^*=2.55$ is the effective principal quantum number for the Cs($5D$) state, and $a_0=0.529$ Å is the Bohr radius.

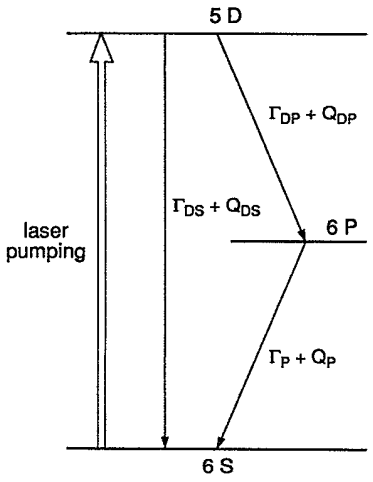

FIG. 8. Simplified energy-level diagram showing processes considered in the analysis of the cascade fluorescence signals. Q's are quenching rates and Γ's are radiative rates.

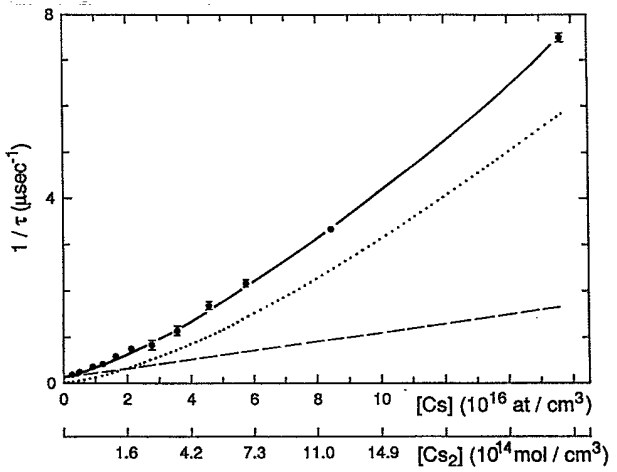

FIG. 9. Dependence of the decay rates for the $6P_{3/2}$ level as a function of atomic and molecular densities. Solid line is the best fit using Eq. (34), while the dotted and dashed lines refer to the molecular and atomic quenching, respectively (the radiative term $\Gamma_{P\text{-eff}}$ has been added to the atomic-quenching contribution).

fluorescence ($\lambda=852.1$ nm). This was because the efficiency of the photomultiplier was low at the wavelength $\lambda=894.3$ nm of the other doublet component, resulting in a reduction of the signal-to-noise ratio.

The density dependence of the slower decay rate was obtained by fitting the late time decay of the time resolved fluorescence with a single exponential. These data are plotted in Fig. 9, which illustrates that, in the range of temperatures explored in our experiment (207–364 °C), the dependence of Γ_P+Q_P on vapor pressure is linear in [Cs] only at low temperatures. At higher temperatures the dimer concentration, which grows faster than [Cs], dominates the quenching of the $6P$ levels. The experimentally observed decay rate of the $6P_{3/2}$ level was therefore fitted to the expression

$$\Gamma_P+Q_P=\Gamma_{P-\text{eff}}+\sigma_P(\text{Cs})\bar{v}_{\text{Cs}-\text{Cs}}[\text{Cs}] +\sigma_P(\text{Cs}_2)\bar{v}_{\text{Cs-Cs}_2}[\text{Cs}_2]\ , \tag{34}$$

where $\sigma_P(\text{Cs})$ and $\sigma_P(\text{Cs}_2)$ are the quenching cross sections for atomic and molecular collisions, and $\bar{v}_{\text{Cs}-\text{Cs}}$ and $\bar{v}_{\text{Cs}-\text{Cs}_2}$ are the mean relative velocities of the two collision partners.

The cross sections obtained from a fit of the data in Fig. 9 are

$$\sigma_P(\text{Cs})=6.6\pm3.0\ \text{Å}^2 \tag{35a}$$

and

$$\sigma_P(\text{Cs}_2)=863\pm260\ \text{Å}^2\ . \tag{35b}$$

The intercept of the decay rate at [Cs]=0 in Fig. 9 gives the inverse trapped lifetime $\tau_{\text{eff}}^{-1}(6P_{3/2})=1.2\times10^5\ \text{s}^{-1}$, which is in reasonable agreement with the value $0.91\times10^5\ \text{s}^{-1}$ calculated from the Holstein theory [37,38] for a cylindrical heat pipe of radius 1.15 cm in the limit where the trapping is dominated by the quasistatic wings.

C. Discussion

The results presented here generally reconcile all previous measurements of the cesium $5D_J$ fine-structure-mixing and out-of-multiplet-quenching rates. They also clearly demonstrate that the $5D$ level quenching is due primarily to ground-state cesium atoms [process (3)]. The results presented here for the mixing and quenching rates are in reasonable agreement (but slightly outside combined experimental uncertainties) with those obtained by Davanloo *et al.* [18].

In Ref. [11], Keramati, Masters, and Huennekens obtained the value $\sigma_{43}=70\pm28\ \text{Å}^2$. This result was based on the assumption that the quenching was molecular [process (4)], and due to the low densities of their experiment, was negligible. Since it is now clear that the quenching is actually atomic, the results of Keramati, Masters, and Huennekens must be reexamined using a model which includes the quenching terms Q_{31}, Q_{32}, Q_{41}, and Q_{42}. The important term here in this context is Q_{41}, which creates additional population in the $6P_{1/2}$ state (the monitored quantity in the experiment of Ref. [11] was I_{10}/I_{20}). In the limit of low density ($\Gamma\gg R,Q$), we find that Eq. (8) reduces to

$$\left[\frac{I_{10}}{I_{20}}\right]^{\text{low density}}_{\text{pump } 5D_{5/2}}=\frac{\epsilon_{10}}{\epsilon_{20}}\frac{\lambda_{20}}{\lambda_{10}}\left[\frac{R_{21}}{\Gamma_{20}}+\frac{\Gamma_{31}}{\Gamma_3}\frac{R_{43}}{\Gamma_4}+\frac{Q_{41}}{\Gamma_4}\right]. \tag{36}$$

This is identical to Eq. (11) of Ref. [11] except for the extra term involving Q_{41}. Thus the quantity actually measured in Ref. [11] was $k_{43}+q_{41}(\Gamma_3/\Gamma_{31})$ rather than simply k_{43}, which those authors reported to be 2.6×10^{-10} $\text{cm}^3\,\text{s}^{-1}$. Using the value of k_{43} measured in the present cw experiment, we find $q_{41}=(1.2\pm1.0)\times10^{-10}\ \text{cm}^3\,\text{s}^{-1}$, which is consistent with the present determinations of the

quenching rates.

In light of these present results, one must also reconsider the published results of Wu and Huennekens [19]. In that work, predissociation and collisional depopulation of the $Cs_2(E)$ states was studied by monitoring the ratio of atomic to molecular fluorescence, as a function of density, following excitation of the molecule with a cw argon-ion laser. The two atomic states that are significantly populated by these mechanisms are $7S$ and $5D$. While quenching of excited atoms by Cs_2 molecules was explicitly considered, and quenching by impurities was discussed at length, quenching by ground-state atoms [process (3)] was neglected. For the $7S$ state, inclusion of such terms would add an additional term $q_{7S}[\mathrm{Cs}]$ to the denominator of the right-hand side of Eq. (18) (of Ref. [19]). This in turn would multiply the right-hand side of Eq. (22) of Ref. [19] by $\Gamma_{7S}/(\Gamma_{7S}+q_{7S}[\mathrm{Cs}])$. If we assume that the $7S$ state atomic quenching is comparable to that reported here for the $5D$ state, then this factor is ~ 1 at low densities and ~ 0.86 at $[\mathrm{Cs}]=3\times 10^{16}$ cm^{-3}. Moreover, such quenching would cause a deviation from linearity of the I_{7S}/I_E-versus-density curve, which was not observed below $[\mathrm{Cs}]=3\times 10^{16}$ cm^{-3} (see Fig. 5a of Ref. 19). Therefore it can be concluded that the $7S$ state results, Γ_{P7S} and k_{7S} of Ref. [19], are correct as printed.

The $5D$ state results of Ref. [19] are more strongly affected by atomic quenching and more difficult to correct due to the possibility that quenching of $7S$ might also populate $5D$. In particular, the inclusion of atomic quenching terms requires that the right-hand side of Eq. (19) of Ref. [19] be replaced by $\{\Gamma_{P5D}+k_{5D}[\mathrm{Cs}] + q_{7S\to 5D}[\mathrm{Cs}][\mathrm{Cs}(7S)] / [\mathrm{Cs}_2(E)]\} / \{\Gamma_{5D} + q_{5D}[\mathrm{Cs}] +k'_{5D}[\mathrm{Cs}_2]\}$. Here, Γ_{P5D} is the rate for predissociation of the $Cs_2(E)$ states to the $5D+6S$ atomic limit, and k_{5D} is the rate coefficient for the process $Cs_2(E) +Cs(6S)\to Cs_2(X)+Cs(5D)$. k'_{5D} is the rate coefficient for the back transfer to the molecule [this is the same as the molecular quenching, process (4), in the present work]. Using the modified version of their Eq. (18) presented above, we obtain a modified version of Eq. (23) of Ref. [19]:

$$\frac{I_{5D}}{I_E}=\frac{\Gamma_{5D\to 6S}}{\Gamma_E}\frac{h\nu_{5D\to 6S}}{h\nu_E}\frac{\epsilon_{5D\to 6S}}{\epsilon_E}\frac{d\Omega_{5D\to 6S}}{d\Omega_E} \times\frac{\Gamma_{P5D}+k_{5D}[\mathrm{Cs}]+q_{7S\to 5D}[\mathrm{Cs}](\Gamma_{P7S}+k_{7S}[\mathrm{Cs}])/(\Gamma_{7S\to 6P}+q_{7S}[\mathrm{Cs}]+k'_{7S}[\mathrm{Cs}_2])}{\Gamma_{5D}+q_{5D}[\mathrm{Cs}]+k'_{5D}[\mathrm{Cs}_2]}. \quad (37)$$

The zero-density intercept of Eq. (37) still yields the predissociation rate (intercept of $I_{5D}/I_E\sim\Gamma_{P5D}/\Gamma_{5D}$) so that Eq. (26) of Ref. [19] and the $5D$ predissociation rates Γ_{P5D} reported in that reference are still correct. However, since the extrapolations to zero density are made from data taken above 10^{16} cm^{-3}, where $q_{5D}[\mathrm{Cs}]$ is still comparable to Γ_{5D}, the reported uncertainties in Γ_{P5D} should be increased; these values are probably only accurate to within a factor of 2.

Because of the complexity of the situation represented by Eq. (37), and the fact that we do not have accurate values for the $7S$ state quenching rates, we must discard the conclusion of Ref. [19] that $k_{5D}<6\times 10^{-11}$ cm^3 s^{-1}. At present, we simply do not have enough information to make any useful statement about the magnitude of k_{5D}, although it is likely to be small since this process is not resonant.

Wu and Huennekens argue that collisional mixing was not occurring among the $5D_J$ sublevels under the conditions of their experiment. Since this conclusion was in error, it was also not correct to report predissociation rates to each $5D_J$ level individually. The values of Γ_{P5D} reported in their Table II are essentially correct as discussed above. However, the values of $\Gamma_{P5D_{3/2}}$ and $\Gamma_{P5D_{5/2}}$ reported there must now also be discarded. The arguments they made to obtain a calibration factor C, which can be used to place the relative photolysis measurements of Refs. [23] and [39] on an absolute scale, are also changed since only the total $5D$ predissociation rate Γ_{P5D} was, in fact, measured. The value they report, 5.8×10^{-18} cm^2, should now be increased to 8.7×10^{-18} cm^2 with the same error bars. In fact, the present results eliminate the apparent discrepancy in the relative $5D_J$ production rates observed in Refs. [19] and [23]. However, it should also be mentioned that the "predissociation rates" presented in Ref. [19] are average values of the dissociation rates of all v,J levels that happen to be pumped by the multimode laser that was used. In fact, the predissociation rates of Ref. [19] were based on total lifetimes measured using the phase-shift technique which assumes single-exponential decay. Recently, Bieniak and Szonert [40] have shown that at least three exponentials are needed to describe the molecular state lifetimes. Again, this points to an averaging over pumped and detected levels and explains Bieniak and Szonert's concern that the Wu-Huennekens predissociation rates are so small. We hope that, using currently available narrow-band lasers, predissociation rates for individual v,J levels will soon be available.

Once we understand that the $5D$ level quenching is predominantly atomic, it is useful to consider how this can come about. The $6P_{3/2}$ state lies 2767 cm^{-1} below the $5D_{3/2}$ level. Quenching of the $5D_J$ levels must occur through a highly repulsive potential curve of the $6P+6S$ manifold. The most likely candidate is the $2\,^3\Sigma_u^+$ state, which according to the most recent calculations by Krauss and Stevens [41] is ~ 2000 cm^{-1} repulsive at $R=11.3$ a.u. A simple extrapolation indicates that the $2\,^3\Sigma_u^+$ state would be 2767 cm^{-1} repulsive near $R=9.5$

a.u.=5.0 Å. Thus a gas-kinetic cross section on the order of $\pi R^2 \sim 80$ Å^2 is possible through this channel. This estimate is not inconsistent with the quenching cross section of ~ 30 Å^2 reported here.

V. CONCLUSIONS

In summary, we have presented the results of a series of pulsed and cw laser experiments designed to study radiative decays and collisional excitation-transfer processes involving the Cs($5D_J$) levels in pure cesium vapor. In particular, we have determined that the principal quenching mechanism of the $5D_J$ levels is atomic in nature [process (3)] as originally implied by Davanloo *et al.* [18]. We have determined absolute magnitudes for both the fine-structure mixing and $5D_J$ out-of-multiplet quenching cross sections with each number being determined from more than one independent technique. Our best values for these cross sections are

$$\sigma_{5D_{5/2}\rightarrow 5D_{3/2}} = \sigma_{43} = 36 \pm 8 \text{ Å}^2 \quad (38)$$

and

$$\sigma_{5D} = \sigma_{3,4} = 30 \pm 3 \text{ Å}^2 . \quad (39)$$

These results are substantially in agreement with the previous results of Davanloo *et al.* [18] (although slightly outside combined error limits) and reconcile the seemingly contradictory results of Refs. [11], [18], and [19]. The mixing rate is also seen to be a factor of 2.9 larger than the geometric cross section (see Table II). This is consistent with the trend observed in Ref. [1] for the higher Cs(nD_J) levels. Specifically, the experimental cross sections were found to agree well with the geometric cross sections for $n=7-10$. However, for $6D$, the experimental value was larger than geometric by a factor of 2.6.

In addition, we have experimentally determined the average natural lifetime of the $5D_J$ levels,

$$\tau_{5D} = 1250 \pm 115 \text{ ns} . \quad (40)$$

From the analysis of the cascading $5D_{3/2,5/2} \rightarrow 6P_{3/2} \rightarrow 6S_{1/2}$ fluorescence we have also determined the $6P_{3/2}$ level quenching cross sections for collisions with Cs_2 molecules

$$\sigma_P(Cs_2) = 863 \pm 260 \text{ Å}^2 \quad (41a)$$

and with Cs atoms

$$\sigma_P(Cs) = 6.6 \pm 3.0 \text{ Å}^2 . \quad (41b)$$

ACKNOWLEDGMENTS

Two of us (A.S. and J.H.) would like to thank the Alexander von Humboldt Stiftung for providing support during our visits. Experimental work at Lehigh University was supported by the National Science Foundation under Grant No. PHY-8451279 and the U.S. Army Research Office under Grant No. DAAL03-89-K-0171. Work at the Universität Kaiserslautern was supported by the Deutsche Forschungsgemeinschaft within the Sonderforschungsbereich 91.

*Permanent address: Dipartimento di Scienze Fisiche dell' Universitá di Napoli, I-80125 Napoli, Italy.

†Present address: Naval Research Laboratory, Optical Sciences Division, 4555 Overlook Avenue S.W., Washington, DC 20375-5000.

[1] A. C. Tam, T. Yabuzaki, S. M. Curry, M. Hou, and W. Happer, Phys. Rev. A **17**, 1862 (1978).
[2] P. Münster and J. Marek, J. Phys. B **14**, 1009 (1981).
[3] J. Wolnikowski, J. B. Atkinson, J. Supronowicz, and L. Krause, Phys. Rev. A **25**, 2622 (1982).
[4] M. Harris and E. L. Lewis, J. Phys. B **15**, L613 (1982).
[5] J. Huennekens and A. Gallagher, Phys. Rev. A **27**, 1851 (1983).
[6] J. W. Parker, H. A. Schuessler, R. H. Hill, Jr., and B. G. Zollars, Phys. Rev. A **29**, 617 (1984).
[7] J. Supronowicz, J. B. Atkinson, and L. Krause, Phys. Rev. A **30**, 112 (1984).
[8] L. Sirko and K. Rosiński, J. Phys. B **18**, L221 (1985).
[9] L. Sirko and K. Rosiński, J. Phys. B **19**, L279 (1986).
[10] J. M. Mestdagh, P. de Pujo, J. Pascale, J. Cuvellier, and J. Berlande, Phys. Rev. A **35**, 1043 (1987).
[11] B. Keramati, M. Masters, and J. Huennekens, Phys. Rev. A **38**, 4518 (1988).
[12] T. R. Mallory, W. Kedzierski, J. B. Atkinson, and L. Krause, Phys. Rev. A **38**, 5917 (1988).
[13] L. J. Kovalenko, S. R. Leone, and J. B. Delos, J. Chem. Phys. **91**, 6948 (1989).
[14] G. C. Schatz, L. J. Kovalenko, and S. R. Leone, J. Chem. Phys. **91**, 6961 (1989).
[15] I. Jackowska and M. Lukaszewski, J. Phys. B **23**, 2097 (1990).
[16] P. W. Arcuni, M. L. Troyer, and A. Gallagher, Phys. Rev. A **41**, 2398 (1990).
[17] L. Krause, in *The Excited State in Chemical Physics,* edited by J. W. McGowan (Wiley, New York, 1975), pp. 267–316.
[18] F. Davanloo, C. B. Collins, A. S. Inamdar, N. Y. Mehendale, and A. S. Naqvi, J. Chem. Phys. **82**, 4965 (1985).
[19] Z. Wu and J. Huennekens, J. Chem. Phys. **81**, 4433 (1984).
[20] M. McClintock and L. C. Balling, J. Quant. Spectrosc. Radiat. Transfer **9**, 1209 (1969).
[21] L. K. Lam, T. Fujimoto, A. C. Gallagher, and M. M. Hessel, J. Chem. Phys. **68**, 3553 (1978).
[22] J. Huennekens and A. Gallagher, Phys. Rev. A **28**, 238 (1983).
[23] C. B. Collins, J. A. Anderson, D. Popescu, and I. Popescu, J. Chem. Phys. **74**, 1053 (1981).
[24] J. Huennekens, H. J. Park, T. Colbert, and S. C. McClain, Phys. Rev. A **35**, 2892 (1987).
[25] T. Colbert and J. Huennekens, Phys. Rev. A **41**, 6145 (1990).
[26] C. G. Carrington, D. N. Stacey, and J. Cooper, J. Phys. B **6**, 417 (1973).
[27] W. R. Hindmarsh and J. M. Farr, Prog. Quantum Electron. **2**, 141 (1973).
[28] A. N. Nesmeyanov, *Vapor Pressure of the Elements*

(Academic, New York, 1964).
[29] L. H. Aller, *Astrophysics–The Atmospheres of the Sun and Stars* (Ronald, New York, 1953).
[30] H. Weickenmeier, U. Diemer, M. Wahl, M. Raab, W. Demtröder, and W. Müller, J. Chem. Phys. **82**, 5354 (1985).
[31] C. R. Vidal and J. Cooper, J. Appl. Phys. **40**, 3370 (1969).
[32] H. Scheingraber and C. R. Vidal, Rev. Sci. Instrum. **52**, 1010 (1981).
[33] R. Castell, W. Demtröder, A. Fischer, R. Kullmer, H. Weickenmeier, and K. Wickert, Appl. Phys. B **38**, 1 (1985).
[34] U. Diemer and W. Demtröder, Chem. Phys. Lett. **176**, 135 (1991).
[35] W. Demtröder, W. Stetzenbach, M. Stock, and J. Witt, J. Mol. Spectrosc. **61**, 382 (1976).
[36] B. Warner, Mon. Not. R. Astron. Soc. **139**, 115 (1968).
[37] T. Holstein, Phys. Rev. **72**, 1212 (1947).
[38] T. Holstein, Phys. Rev. **83**, 1159 (1951).
[39] C. B. Collins, F. W. Lee, J. A. Anderson, P. A. Vicharelli, D. Popescu, and I. Popescu, J. Chem. Phys. **74**, 1067 (1981).
[40] B. Bieniak and J. Szonert, Phys. Lett. A **152**, 47 (1991).
[41] M. Krauss and W. J. Stevens, J. Chem. Phys. **93**, 4236 (1990).
[42] M. Fabry, J. Quant. Spectrosc. Radiat. Transfer **16**, 127 (1976).
[43] P. M. Stone, Phys. Rev. **127**, 1151 (1962).
[44] O. S. Heavens, J. Opt. Soc. Am. **51**, 1058 (1961).
[45] C. E. Theodosiou, Phys. Rev. A **30**, 2881 (1984).
[46] J. Marek, J. Phys. B **10**, L325 (1977).
[47] H. Bethe and E. E. Salpeter, in *Handbuch der Physik*, edited by S. Flügge (Springer-Verlag, Berlin, 1957), Vol. XXXV, pp. 88–436.